CHEMISTRY
A European Journal

Supporting Information

# Enhancing the Viscosity-Sensitive Range of a BODIPY Molecular Rotor by Two Orders of Magnitude**

Stepas Toliautas,[b] Jelena Dodonova,[c] Audrius Žvirblis,[a] Ignas Čiplys,[a] Artūras Polita,[a] Andrius Devižis,[a] Sigitas Tumkevičius,[c] Juozas Šulskus,[b] and Aurimas Vyšniauskas*[a]

chem_201901315_sm_miscellaneous_information.pdf

**Table of Content**

## 1. Spectroscopic characterisation, fluorescence lifetime measurements

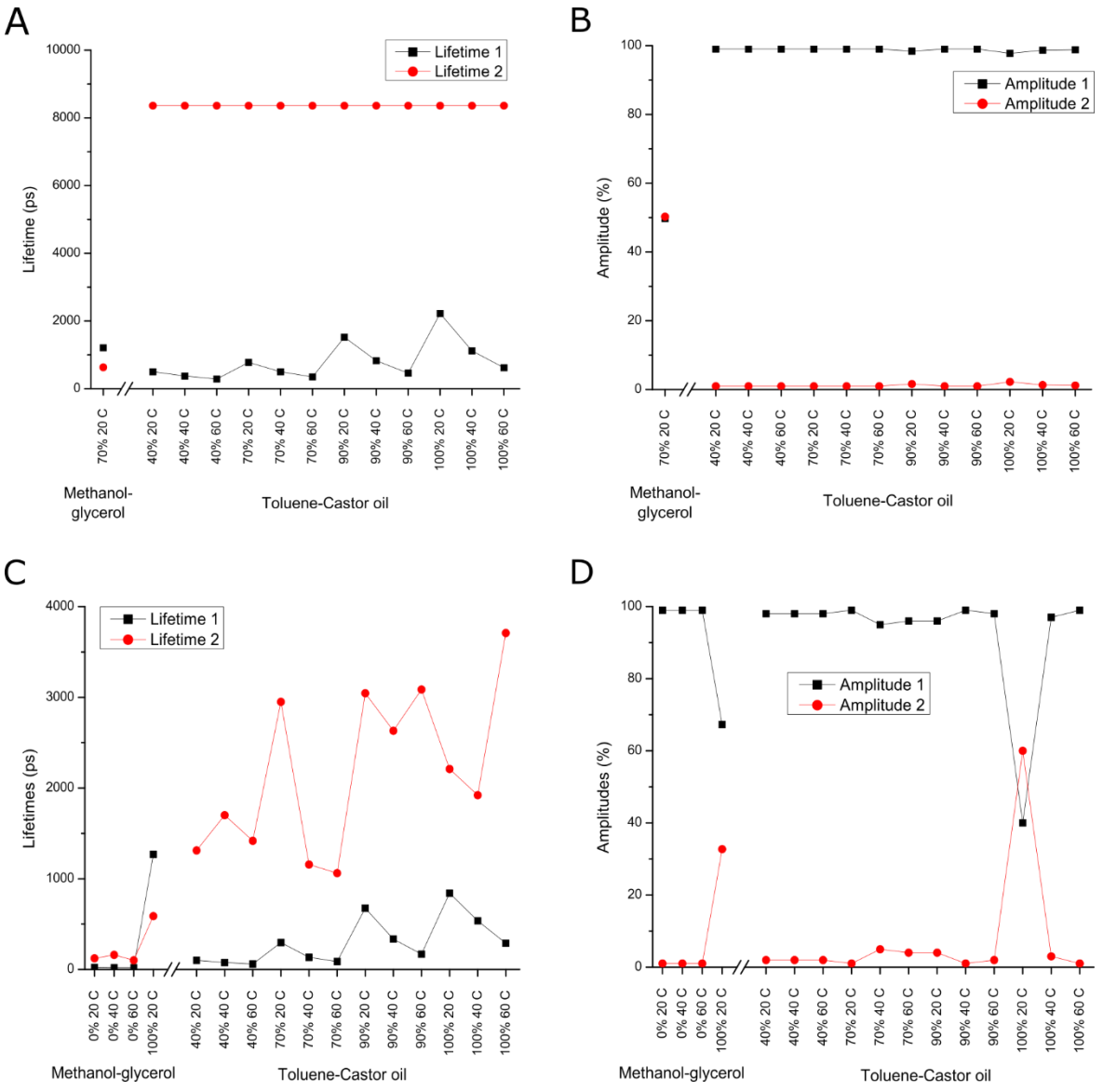


**Figure S1**. Individual lifetimes and amplitudes of **BDP-H** (A, B) and **BDP-NO$_2$** (C, D). These values were used for calculating intensity-weighted average lifetimes on instances where monoexponential fitting was not sufficient. The intensity-weighted average lifetimes are shown in the main text, Figures 2 and 3C. Fluorescence decays of **BDP-H** in toluene-Castor oil mixtures had a small contribution (< 3% by amplitude) from fluorescence of Castor oil. Therefore, one lifetime component was fixed to 8363 ps (the average fluorescence lifetime of Castor oil) and not used for calculating intensity-weighted mean lifetime. For **BDP-NO$_2$**, in multiple cases a longer lifetime component was observed possessing insignificant amplitude (< 5%), likely to come from Castor oil as well. The lifetime of this component was smaller than 8363 ps most likely due to narrower time window, which captures only a part of a decay of the Castor oil fluorescence. In all instances, if the small amplitude component was below 10 %, it was not used for calculating intensity-weighted mean lifetime, because then it is possible to confidently separate the fluorescence of the fluorophore from contributions from Castor oil or impurities.

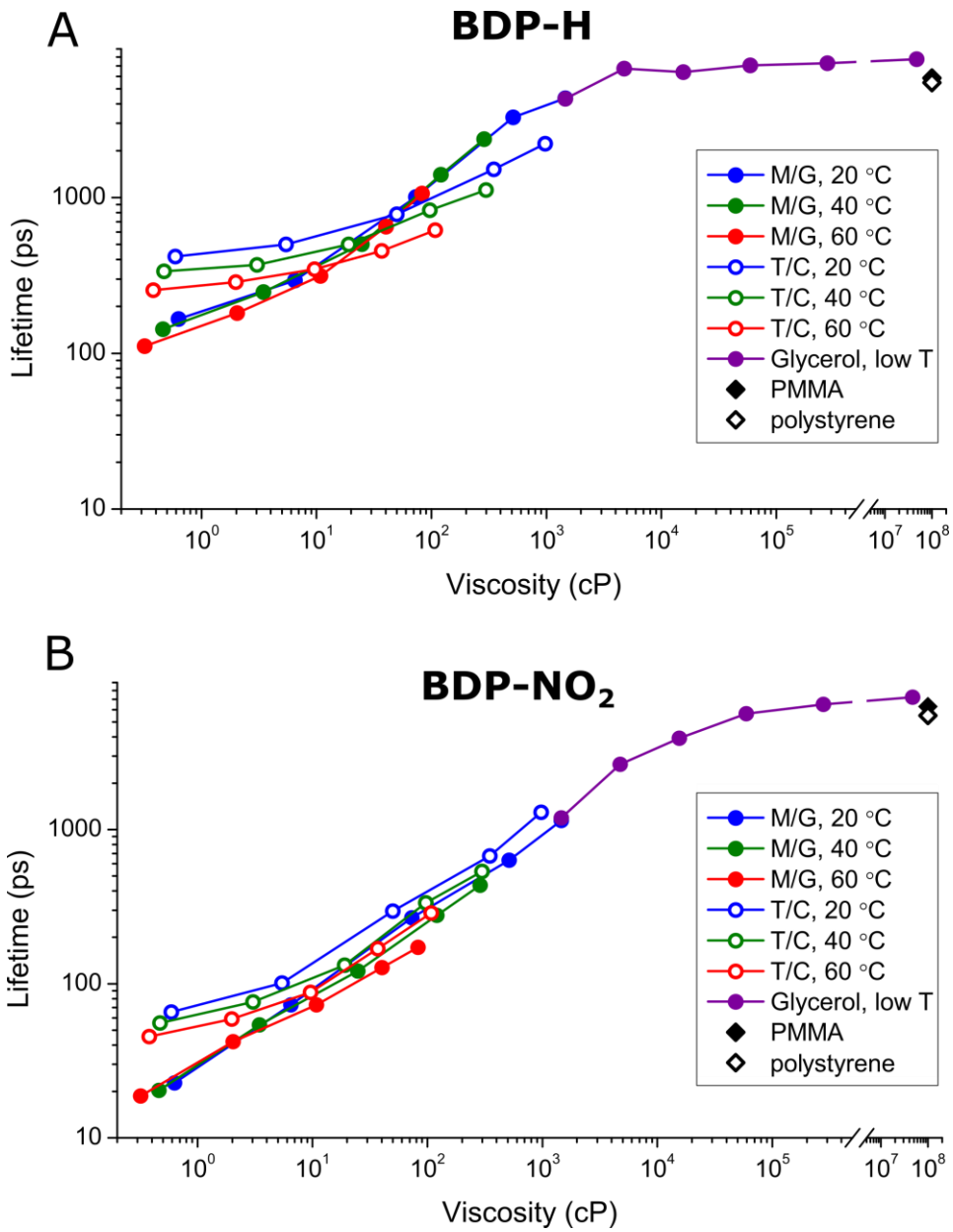


**Figure S2**. The full set of fluorescence lifetime data of and **BDP-H** (A) and **BDP-$NO_2$** (B). The lifetimes were measured in methanol-glycerol and toluene-Castor oil mixtures at 20 ˚C, 40 ˚C, and 60 ˚C, in cooled glycerol, and in polymers (PMMA and polystyrene) at room temperature. The lifetimes obtained in polymers were slightly lower than the lifetimes in glycerol at low temperature (down to 225 K), most likely due to faster non-radiative relaxation at higher temperature.

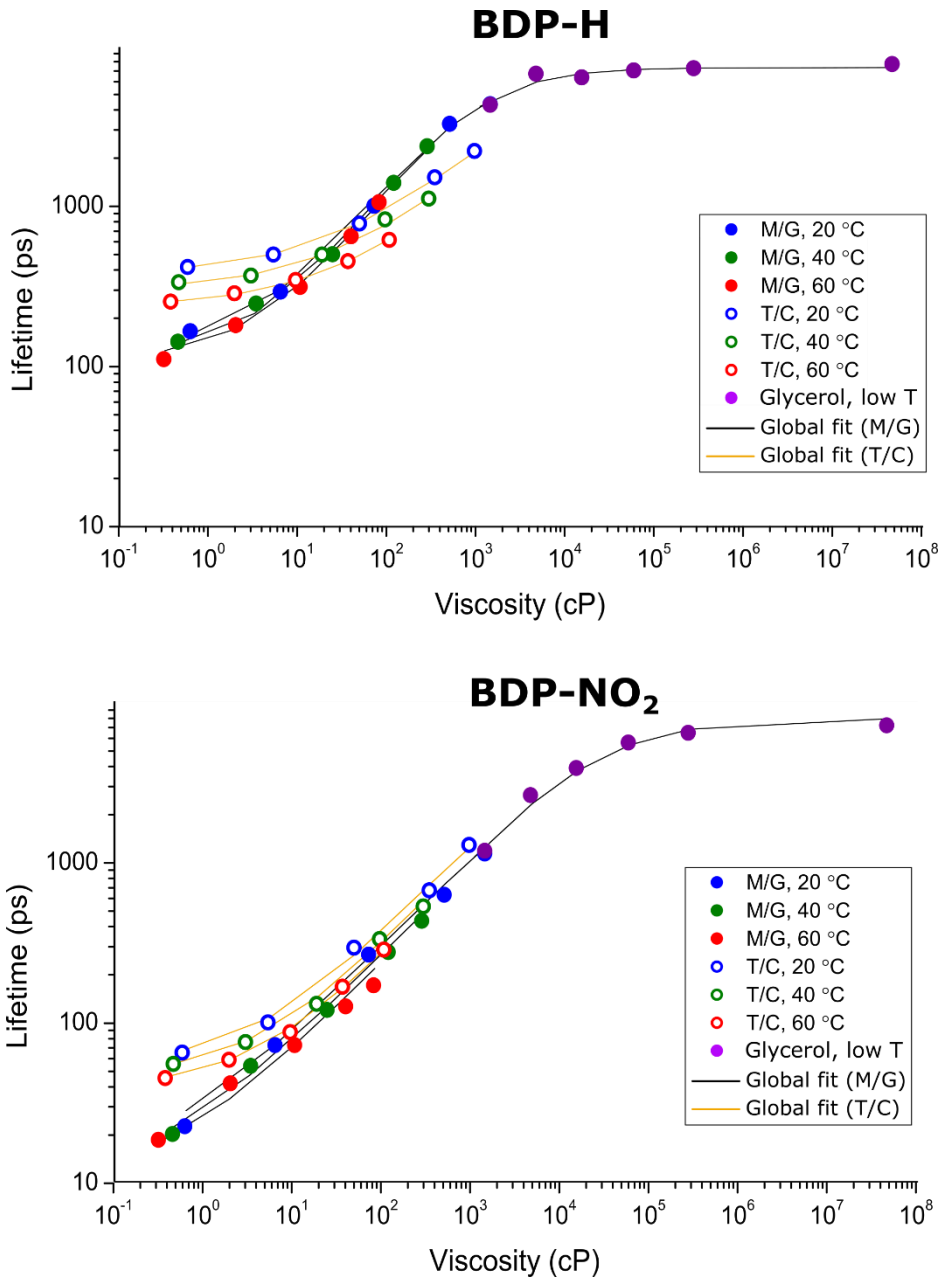


**Figure S3**. Global fits of lifetimes of **BDP-H** and **BDP-NO$_2$**. Two global fits for each dye are shown; one for data measured in methanol-glycerol mixtures and pure glycerol at varying temperature, another for toluene-Castor oil mixtures. Equation (1) (main text) was used as a basis for the fitting function:

$$\tau = \frac{1}{\frac{1}{a_1\eta^{a_2} + a_3} e^{a_4/T} + a_5}$$

where $\tau$ is fluorescence lifetime, $\eta$ is viscosity, $T$ is temperature, and $a_{1\ldots5}$ are fitting parameters. The fitting parameters obtained are shown in Table S1.

**Table S1**. Obtained fitting parameters from the fits in Figure S3. The errors specify 90% confidence interval.

| | Solvent mixture | $a_1$ | $a_2$ | $a_3$ | $a_4$ | $a_5$ |
|---|---|---|---|---|---|---|
| **BDP-NO$_2$** | Methanol-glycerol | 2.6 ± 2.9 | -0.58 ± 0.05 | 1.5 ± 2.1 | (0.60 ± 0.37) $\cdot 10^3$ | (1.3 ± 0.2) $\cdot 10^{-4}$ |
| | Toluene-Castor oil | 1.0 ± 0.8 | -0.65 ± 0.09 | 3.2 ± 2.2 | (0.83 ± 0.21) $\cdot 10^3$ | (1.7 ± 2.6) $\cdot 10^{-4}$ |
| **BDP-H** | Methanol-glycerol | 13 ± 11 | -0.76 ± 0.06 | 36 ± 31 | (0.37 ± 0.26) $\cdot 10^3$ | (1.3 ± 0.1) $\cdot 10^{-4}$ |
| | Toluene-Castor oil | 0.84 ± 0.53 | -0.56 ± 0.08 | 6.6 ± 2.7 | (1.2 ± 0.1) $\cdot 10^3$ | (1.0 ± 1.1) $\cdot 10^{-5}$ |

The fitting parameters are related to the following important photophysical parameters for **BDP-NO$_2$** and **BDP-H**: parameter $x$ ($x = -a_2$) defining the fluorophore's sensitivity to viscosity and theoretically predicted to be between 0 and 1, maximum non-radiative decay rate $k_{nr,max}$ ($k_{nr,max} = 1/a_3$) achievable at infinite temperature and 0 cP viscosity, activation energy barrier $E_a$ ($E_a = a_4 \cdot 8.314 \text{J/(K·mol)}$) leading to temperature-dependent fluorescence lifetime, and maximum achievable fluorescence lifetime $\tau_{max}$ ($\tau_{max} = 1/a_5$) at infinite viscosity and 0 K temperature.

The large errors of the parameters $a_1$ and $a_3$ are caused by the fact that the increase of one parameter can be compensated by the decrease of another and *vice versa*. The large error of $a_5$ in toluene-Castor oil mixtures is caused by the lack of high viscosity data.

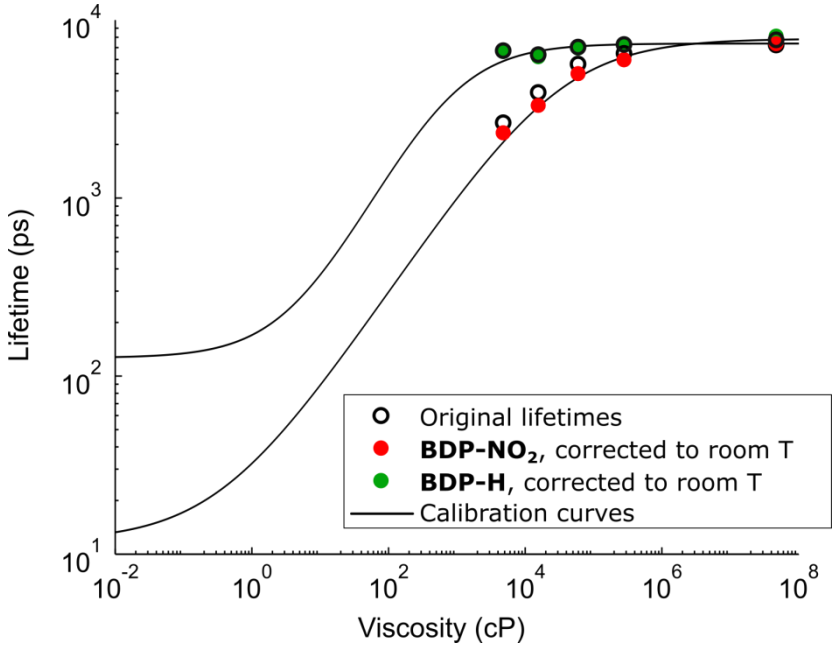


**Figure S4**. Calculated fluorescence lifetimes of **BDP-NO$_2$** and **BDP-H** in hypothetical room temperature (20 ˚C) and very high viscosity conditions. The original lifetimes obtained in cooled glycerol are shown as black circles. In order to achieve a better comparison of data obtained over a wide viscosity range, the obtained lifetimes in cold glycerol were recalculated to expected lifetimes at same viscosity, but at room temperature. The resulting lifetimes are shown as red and green filled circles. Recalculation was done using the fitting function and the parameters obtained in the global fits shown in Figure S3 and Table S1. The recalculated lifetimes of **BDP-NO$_2$** were slightly reduced due to the increase in the non-radiative relaxation rate from the fluorescent state at higher temperature. In contrast, the recalculated lifetimes of **BDP-H** did not show any difference from the original lifetimes, because at these viscosities temperature-dependent non-radiative relaxation of **BDP-H** is much slower than the temperature-independent radiative relaxation.

## 2. Femtosecond transient absorption

Previous studies of **BDP-H**[1] revealed that upon excitation the rotor relaxes from Franck-Condon (FC) state to the local minimum with as reflected by ~10 ps lifetime component and then the rotor leaves the fluorescent state and quickly returns to the ground state, which is revealed as a ~400 ps component in both stimulated emission (SE) and ground state bleach (GSB) bands. Since the ~400 ps components were found in both GSB and SE bands, it means that **BDP-H** does not enter any long-lived intermediate states upon leaving the fluorescent state and returns to the ground state either via a conical intersection or a very fast internal conversion. Additionally, a short (~1 ps) component was also present in the GSB band. In the light of these previously obtained results, we have tested if **BDP-NO$_2$** follows similar mechanism upon excitation. The obtained transient absorption spectra are shown in Figure 4 (main text) and Figure S5.

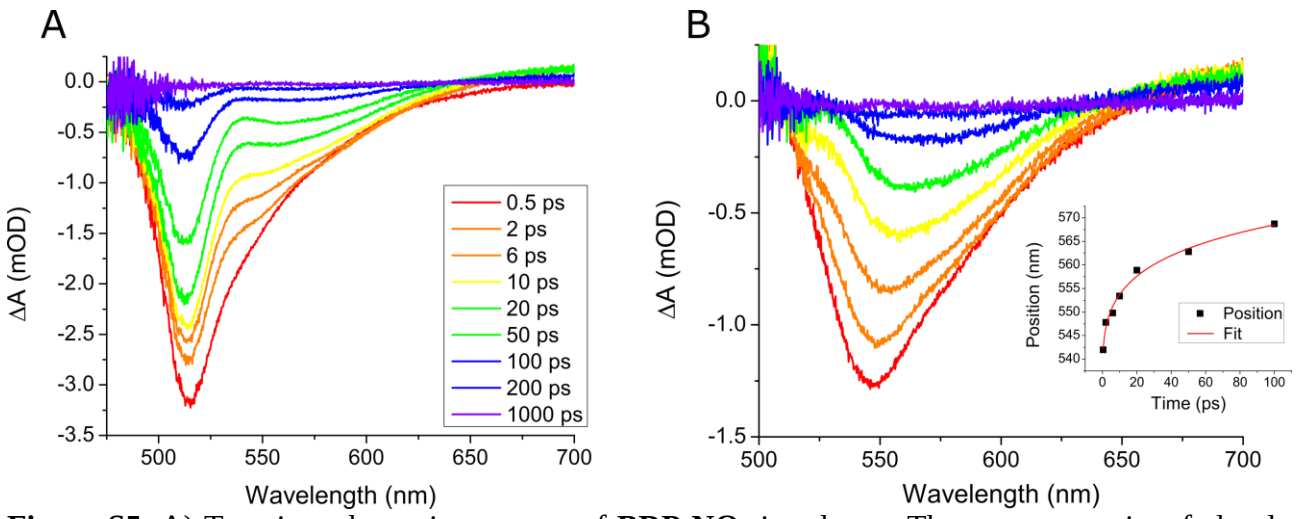


**Figure S5.** A) Transient absorption spectra of **BDP-NO$_2$** in toluene. The spectra consist of closely overlapping ground state bleach (GSB) and stimulated emission (SE) bands. B) Transient absorption spectra with the GSB spectra subtracted, which reveals pure SE band (525-600 nm). The shift of the position of the SE band with time is shown in the inset.

The first observation is that in 1000 ps after excitation all features in transient absorption spectra are gone, which means that **BDP-NO$_2$** is fully relaxed and does not enter any long-lived states, such as a triplet state. The transient absorption spectra reveal closely overlapping GSB and SE bands. The most intense peak in the transient absorption spectra mostly belongs to the GSB band, since its peak at 515 nm is not far from the absorption maximum of **BDP-NO$_2$** in toluene (511 nm, Table 1, main text). The SE band is located at 540-600 nm; it becomes easily visible and slightly separated from the GSB band at delay times of 20 ps and above. In order to visualize the shift of the SE band clearly, we have subtracted the absorption spectra of **BDP-NO$_2$** in toluene from the transient absorption spectra; the result is shown in Figure S5B. The shift is almost completed in 50 ps after excitation (see inset, Figure S5B) and is likely to be caused by relaxation from the Franck-Condon (FC) state to a local minimum. While the SE band shifts, the molecule also leaves the fluorescent state while evolving, as revealed by the quick decrease in the intensity of the transient absorption spectra. Since the shift of the SE band complicates global fitting of the whole set of spectra, we have globally fitted only the GSB band (500-520 nm). Two exponential components were obtained – a short ~0.8 ps component, also observed for **BDP-H** previously[1], and a longer 81 ps component; the fit at 510 nm is shown in the Figure S6 as an example. The GSB band is dominated by the 81 ps component, which is close to the fluorescence lifetime of **BDP-NO$_2$** in toluene (65 ps). The closeness of both lifetimes means that **BDP-NO$_2$** relaxes to the ground state immediately after leaving the fluorescent state. Therefore, the transient absorption data do not provide any evidence on other long-lived states besides the fluorescent state.

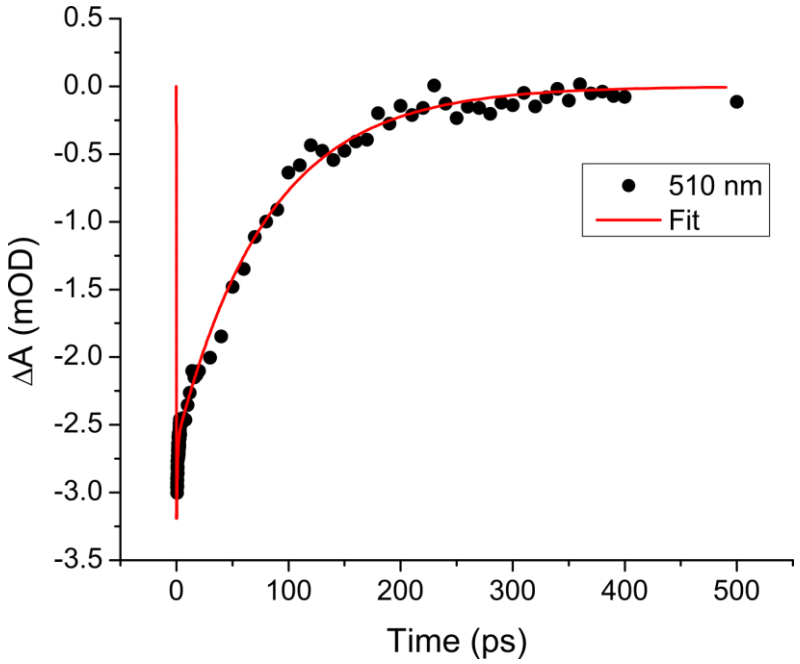


**Figure S6**. Transient absorption data of **BDP-NO$_2$** in toluene at 510 nm, which is the center part of the ground state bleach band. The fit (red line) provides 0.8 ps and 81 ps lifetimes.

## 3. Quantum chemical calculations

Main optical properties of the BODIPY compounds obtained from theoretical calculations are summarized in Table S2. Calculated transition energy values are approximately by 0.4 eV larger than the ones obtained from the absorption and fluorescence spectra. However, the calculations correctly predict lower energy gap and higher Stokes shift for **BDP-NO$_2$**. Both the systematic energy shift and good linear correlation with experimental results are common for the TD-DFT calculations in general and for similar specific compounds.[2]

**Table S2**. The energy of the first electronic transition ($\Delta E$) and corresponding oscillator strengths ($f$) at the $S_{0,\,m}$ (the ground state minimum) and $S_{1,\,m}$ (the excited state local minimum from where fluorescence takes place) geometries of the BODIPY-based compounds.

| | | **$S_{0,\,m}$** | | **$S_{1,\,m}$** | |
|---|---|---|---|---|---|
| | | *Calc.* | *Exp.* | *Calc.* | *Exp.* |
| **BDP-H** | $\Delta E$ (eV) | 2.91 | 2.47 | 2.77 | 2.37 |
| | $f$ | 0.57 | - | 0.51 | - |
| **BDP-NO$_2$** | $\Delta E$ (eV) | 2.86 | 2.44 | 2.65 | 2.27 |
| | $f$ | 0.56 | - | 0.47 | - |

Since the femtosecond transient absorption data suggest that **BDP-H** and **BDP-NO$_2$** relax rapidly to the ground state upon leaving the fluorescence state, we have attempted to locate the intersection point of ground and first excited electronic states, through which rapid relaxation is likely to take place. Minimizing the energy of the first excited electronic state for the different values of the dihedral angle ($\Theta$) does not directly lead to an intersection point between the ground and the first excited state. Therefore, to evaluate a possibility for such an intersection to exist, other structural degrees of freedom constituting the potential energy (hyper)surface of the molecule have to be considered, such as a commonly-used out-of-plane bend angle of the BODIPY core, ($\omega$).[3] Results of calculations performed after changing this angle from the starting structure of $S_{1,r}$ (Figure 5C, main text) are shown in Figure S7. The $S_0$-$S_1$ energy gap is drastically reduced when the angle reaches 110-105°. This signals the existence of the nearby state-crossing point (for instance, avoided crossing or the conic intersection, as suggested by Prlj et al.[4]) that enables non-radiative relaxation and facilitates the return of the dye back to the ground state. Even though TD-DFT becomes unreliable when the energy gap between electronic states becomes small, the discovered geometry is quite similar to the one previously obtained by Prlj *et al.* using specific computational methods for finding intersections of the potential energy surfaces.

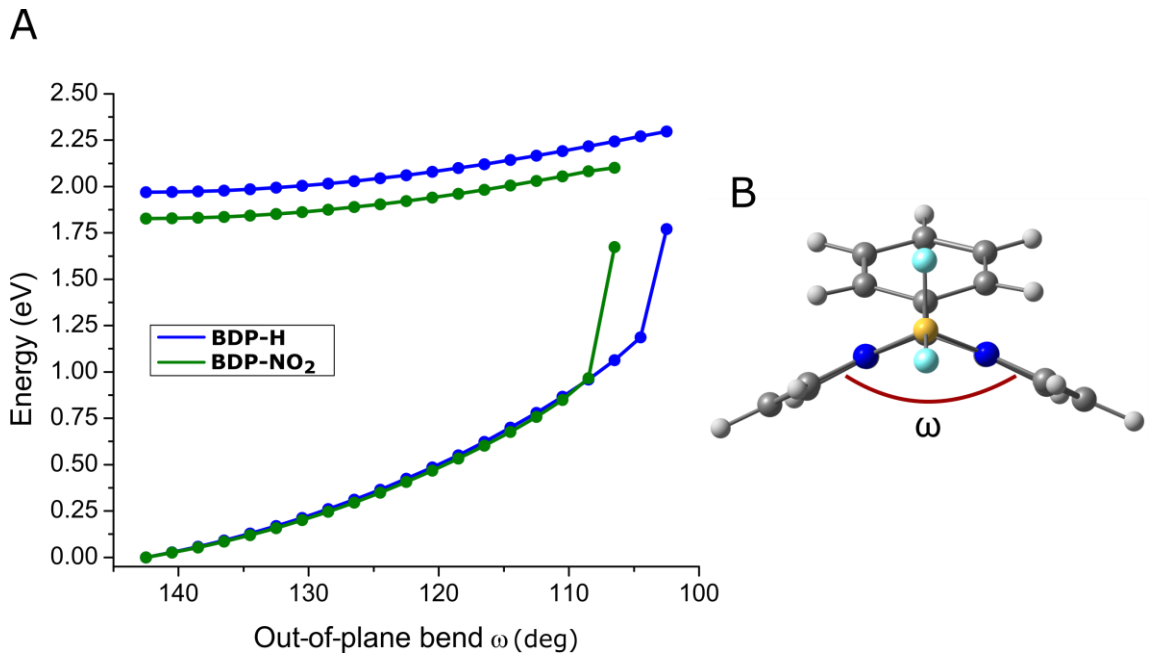


**Figure S7**. Vicinity of the crossing point of the ground and excited electronic states near the excited state minimum of **BDP-H** and **BDP-NO$_2$**. A) The energy dependence of the investigated fluorophores in the ground and excited state on the out-of-plane bend angle. The angle is shown in B).

The leading component of the single-electron transition contributions to the energy of the lowest electronic excitation of BODIPY-based compounds was found to be HOMO-LUMO transition. The calculated properties of frontier molecular orbitals are provided in Table S3 and Figure S8. While the energy of the HOMO is relatively stable for the different geometric structures under consideration and only changes when the BODIPY core itself is deformed, the energy of the LUMO exhibits marked dependence on the dihedral angle ($\Theta$). Moreover, in the case of the **BDP-NO$_2$** compound the energy of the LUMO is lowered 50 % more compared to **BDP-H** when $\Theta$ reaches 0°. Stabilization of the $S_1$ electronic state that follows from these results is the key factor that drives the fluorophores to rotate upon excitation.

**Table S3**. Energies (eV) of HOMO and LUMO of **BDP-H** and **BDP-NO$_2$** at *0°* and *90°* dihedral angles and at dihedral angle corresponding to $S_{1,m}$ geometry (Figure 5C). The energy values are shown with respect to the lowest energy value for each orbital. The resulting difference between orbital energies at *0°* and *90°* angles ($\Delta E_{90°-0°}$) is provided for easier comparison.

| | | Dihedral angle $\theta$ | | | $\Delta E_{90°-0°}$ |
|---|---|---|---|---|---|
| | | *0°* | *~45°* ($S_{1,m}$) | *90°* | |
| **BDP-H** | *HOMO* | 0.27 | 0 | 0.01 | 0.26 |
| | *LUMO* | 0 | 0.45 | 0.54 | 0.54 |
| **BDP-NO$_2$** | *HOMO* | 0.24 | 0 | 0.01 | 0.23 |
| | *LUMO* | 0 | 0.53 | 0.82 | **0.82** |

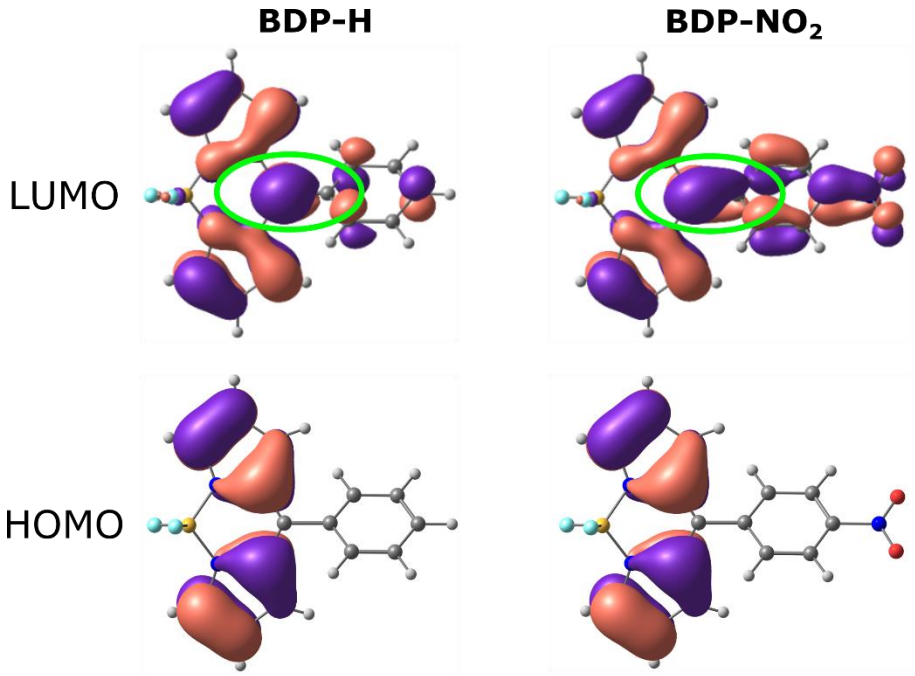


**Figure S8**. The shapes of HOMO and LUMO of **BDP-H** and **BDP-NO$_2$** at the $S_{1,m}$ geometry (Figure 5C, main text). HOMO is fully localized on the BODIPY core and has a nodal plane along the center of the fluorophores. As a result, the energy of HOMO is barely sensitive to the changes of the dihedral angle, as shown in the Table S3. In contrast, LUMO shows an appreciable electron density on the phenyl ring; it also has bonding character along the bond connecting the phenyl ring to the BODIPY core, as highlighted by a green oval. When the dihedral angle is reduced, the overlap of *p* orbitals along the central bond increases reducing the energy of the LUMO. Also, it can be clearly seen that the electron density along the central bond is greater for **BDP-NO$_2$**, which is the reason for the greater change of LUMO energy when the dihedral angle decreases.

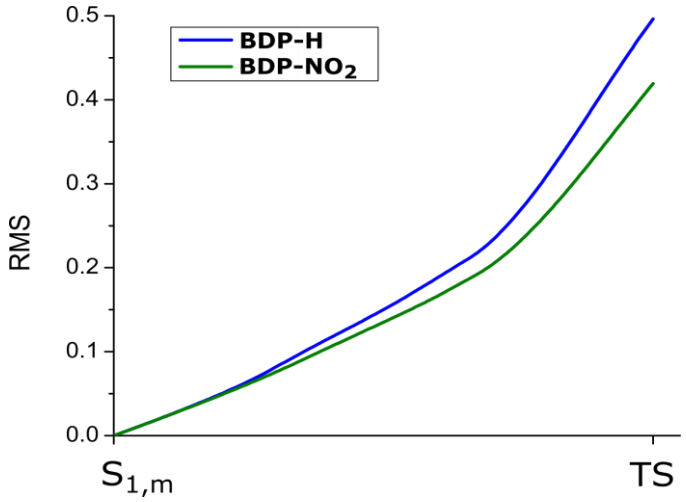


**Figure S9**. Cumulative change of atomic coordinates of **BDP-H** and **BDP-$NO_2$** fluorophores during rotation out of the fluorescent minimum in the $S_1$ state ($S_{1,m}$) to the top of the energy barrier (TS). The *y* axis tracks relative differences in atomic coordinates compared to the $S_{1,m}$ structure. **BDP-$NO_2$** changes its geometry to a lesser degree than **BDP-H**, which is likely to additionally contribute to its faster relaxation from the fluorescent state at equal viscosity conditions (cf. main text).

## 4. Synthesis and NMR spectra of BDP-H and BDP-$NO_2$

**Reaction scheme**

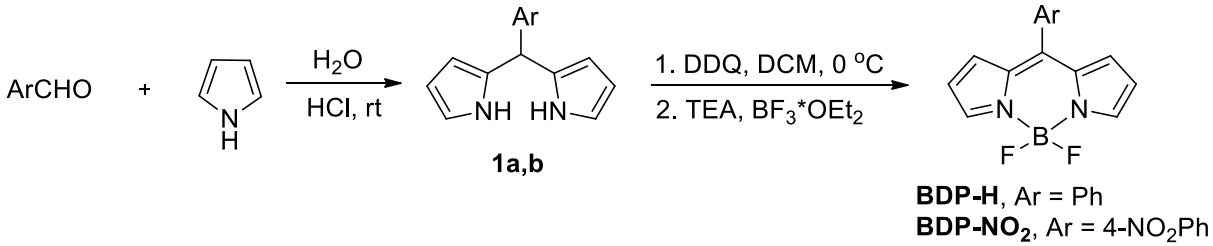


**General procedure for the synthesis of aryldipyrromethanes 1a, b**

Pyrrole (3 equiv.) was added to 100 mL of 0.18 M aqueous HCl (1.5:98.5), followed by the addition of the appropriate aromatic aldehyde (1 equiv., 0.01 mol). The reaction mixture was stirred at room temperature and the reaction progress was monitored by Thin Layer Chromatography (TLC). After the indicated time, the precipitated (semi-) solid product was filtered off and washed with water and petroleum ether to afford aryldipyrromethanes **1a,b**. 5-phenyldipyrromethane (**1a**) and 5-(4-nitrophenyl)dipyrromethane (**1b**) were characterized by their melting point and NMR ($^1$H) spectra and showed the same values as those reported in literature.[5–7]

**5-Phenyldipyrromethane (1a).** Synthesized following the aforementioned procedure, reaction time 4 h. Pale yellow crystals: mp 103-104 °C. Yield: 1.63 g (75%). $^1$H NMR ($CDCl_3$): δ (ppm) = 7.91 (br s, 2H), 7.24-7,38 (m, 5H), 6.72 (s, 2H), 6.20 (d, *J* = 4.0 Hz, 2H), 5.96 (s, 2H), 5.50 (s, 1H).

**5-(4-nitrophenyl)dipyrromethane (1b).** Synthesized following the aforementioned procedure, reaction time 2 h. Bright yellow crystals: mp 160-161 °C. Yield: quantitative. $^1$H NMR ($CDCl_3$): δ

(ppm) = 8.19 (d, $J$ = 8.0 Hz, 2H), 8.02 (br s, 2H), 7.39 (d, $J$ = 8.0 Hz, 2H), 6.77-6.78 (m, 2H), 6.21 (q, $J$ = 4.0 Hz, 2H), 5.89-5.91 (m, 2H), 5.61 (s, 1H).

**General Procedure for the Preparation of the BDP-H and BDP-$NO_2$**

BODIPYs were synthesized by the analogical procedure as in ref.[8] DDQ (150 mg, 0.66 mmol) was slowly added to a flask containing appropriate pyrromethane **1a** or 1**b** (0.6 mmol) in DCM (20 mL) cooled in an ice bath. The reaction mixture was stirred at this temperature for 20 min before triethylamine (0.6 mL) and $BF_3{\cdot}Et_2O$ (0.6 mL) were quickly added to the reaction mixture. The reaction was further stirred at room temperature for 2 h and extracted with DCM (3x40 mL). The organic layers were combined, washed with water (2x 100 mL), dried with anhydrous $Na_2SO_4$, and then the solvent was removed under reduced pressure. The crude product was further purified by column chromatography on silica gel using DCM as the eluent to give the desired BODIPYs as reddish powders. BODIPYs were characterized by melting point and NMR ($^1$H, $^{11}$B, $^{19}$F) spectra and showed essentially the same values as those reported in literature.[9]

**BDP-H.** Yield: 64 mg (40%). Mp 105-106 °C. $^1$H NMR ($CDCl_3$): δ (ppm) = 7.97 (s, 2H), 7.543-7.63 (m, 5H), 6.96 (d, $J$ = 4 Hz, 2H), 6.57 (d, $J$ = 4 Hz, 2H). $^{11}$B NMR ($CDCl_3$): δ = -0.29 (t, $J_{av}$ = 28.9 Hz). $^{19}$F NMR ($CDCl_3$): δ = -144.98 (q, $J_{av}$ = 30.1 Hz).

**BDP-$NO_2$.** Yield: 70 mg (20%). Mp 277-278 °C (lit. 277-278 °C). $^1$H NMR ($CDCl_3$): δ (ppm) = 8.44 (d, $J$ = 8.0 Hz, 2H), 8.03 (s, 2H), 7.79 (d, $J$ = 8.0 Hz, 2H), 6.87 (s, 2H), 6.62 (s, 2H). $^{11}$B NMR ($CDCl_3$): δ = -0.76 (t, $J_{av}$ = 28.2 Hz). $^{19}$F NMR ($CDCl_3$): δ = -144.93 (q, $J_{av}$ = 30.1 Hz).

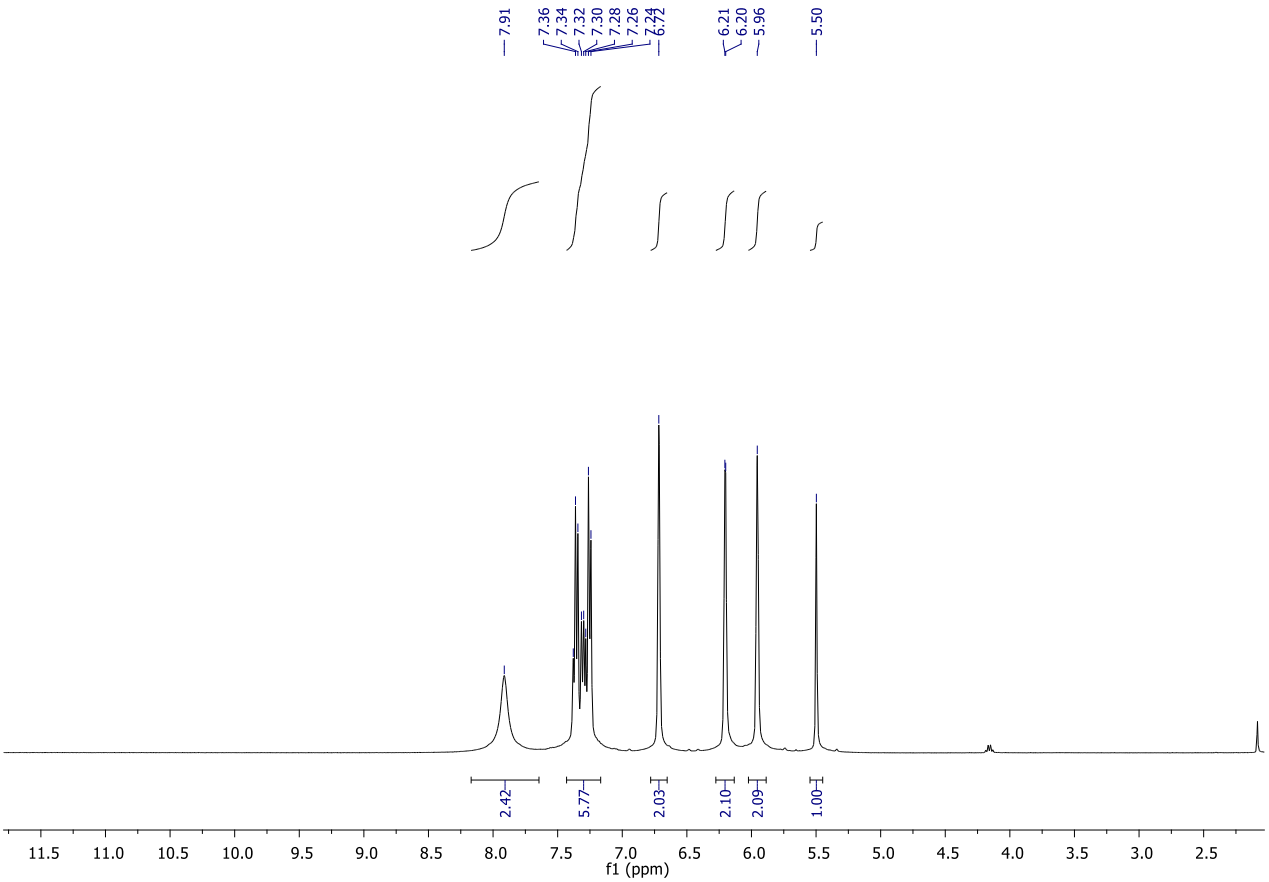


**Figure S10.** $^1$H NMR spectrum of **1a**.

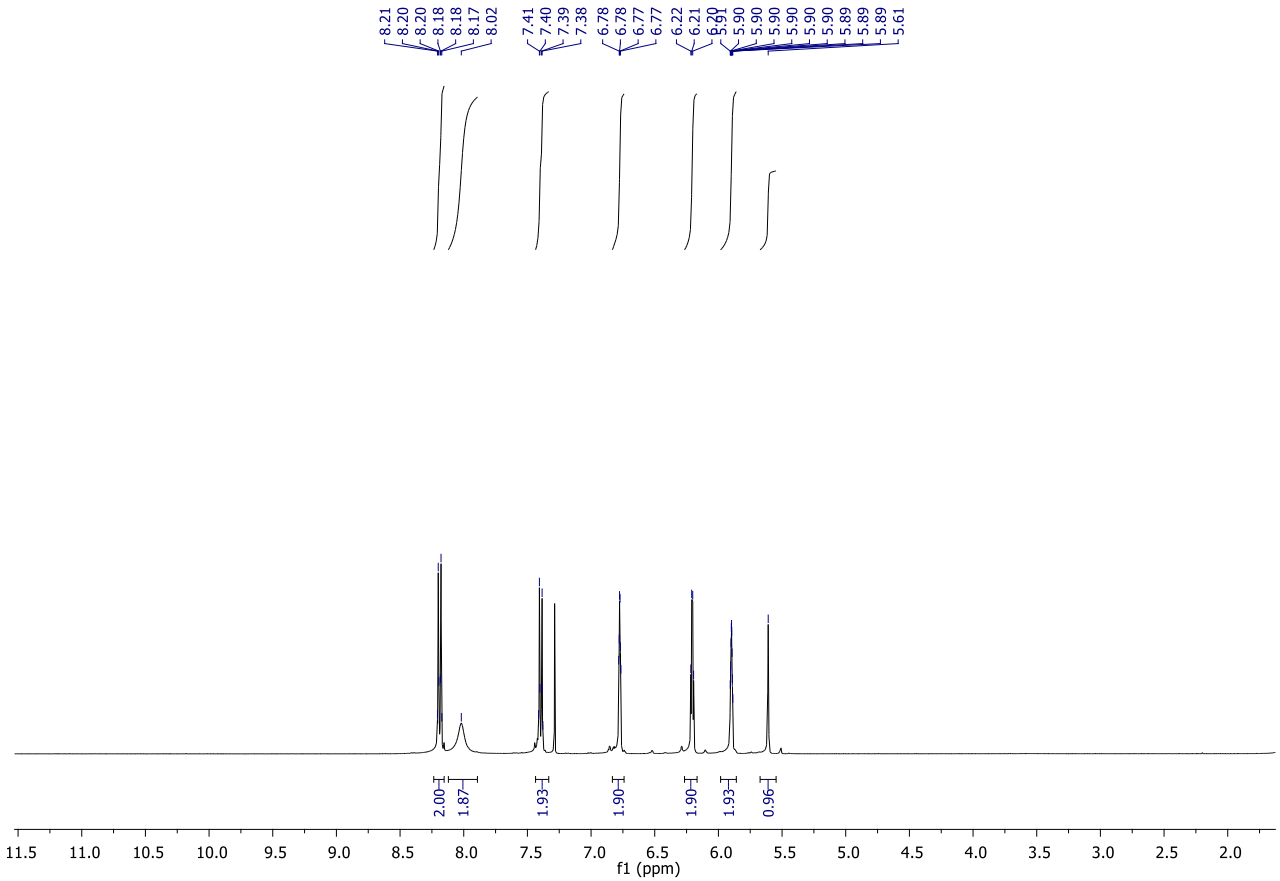


**Figure S11.** $^{1}$H NMR spectrum of **1b**.

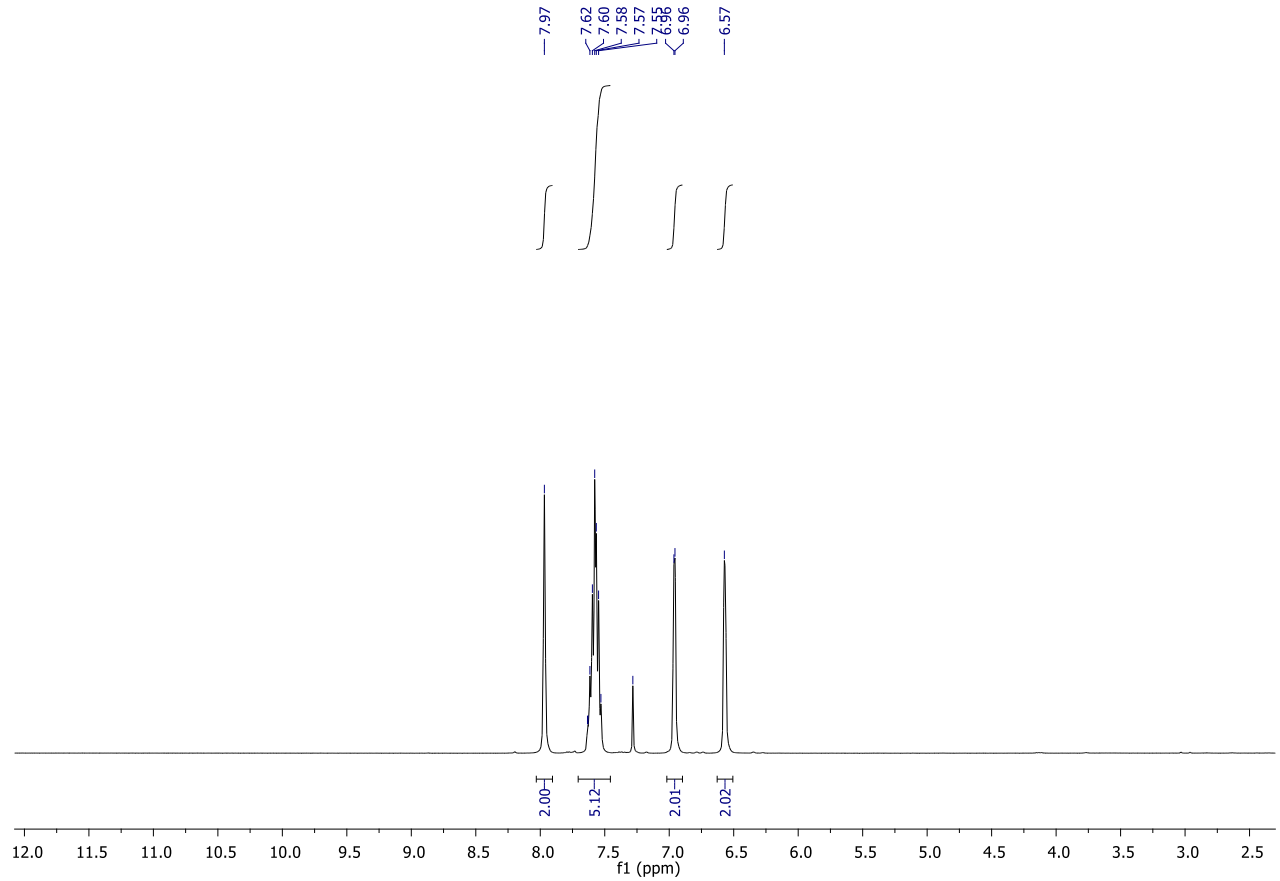


**Figure S12.** $^{1}$H NMR spectrum of **BDP-H**.

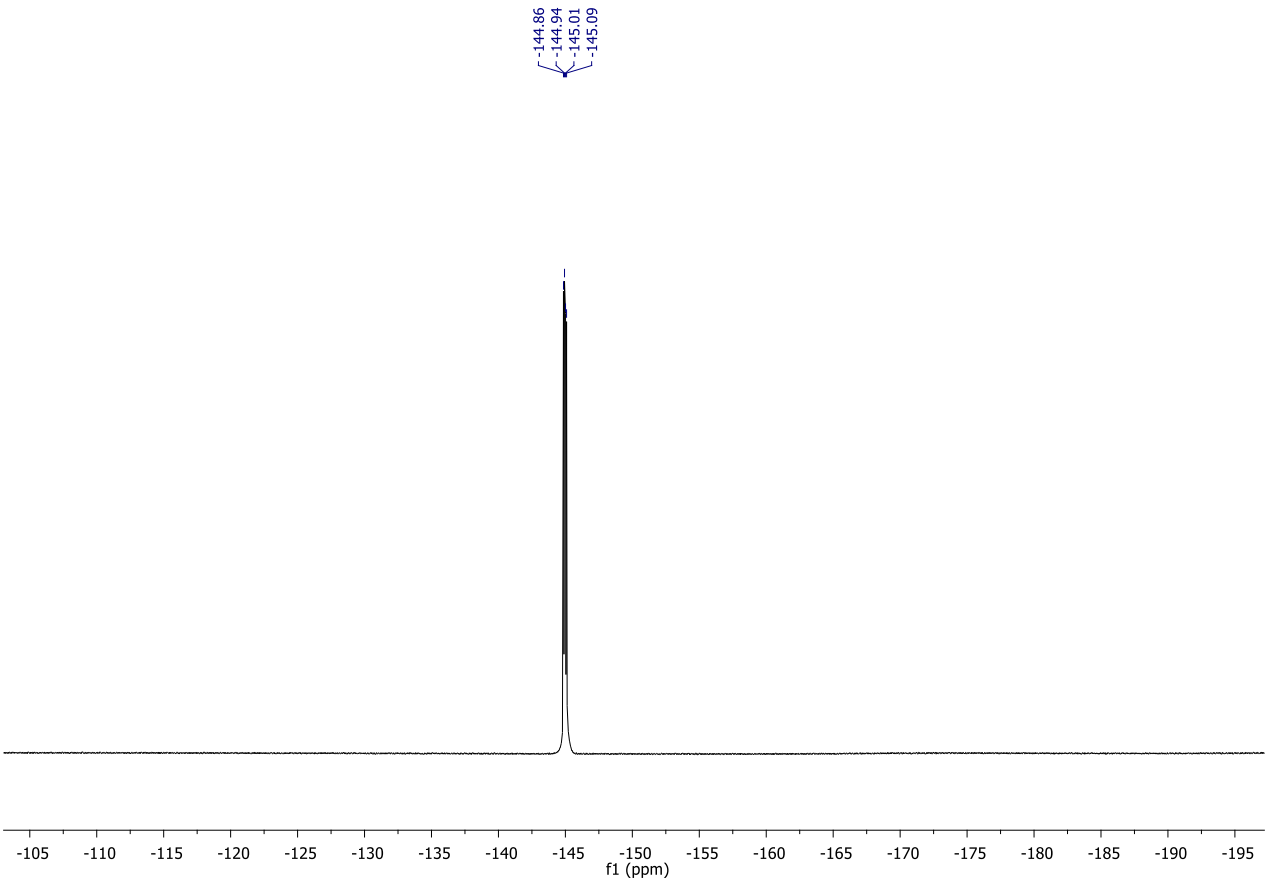


**Figure S13.** $^{19}$F NMR spectrum of **BDP-H**.

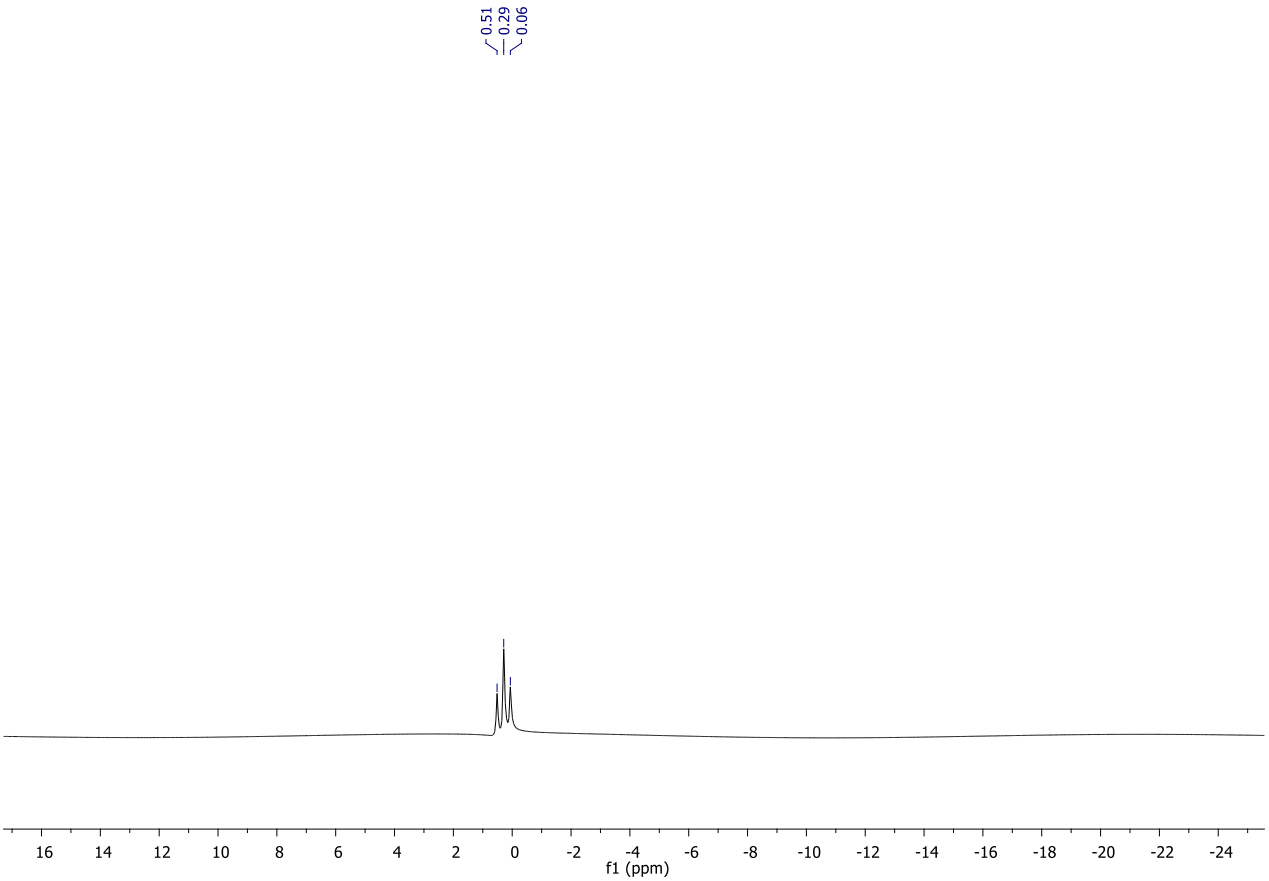


**Figure S14.** $^{11}$B NMR spectrum of **BDP-H**.

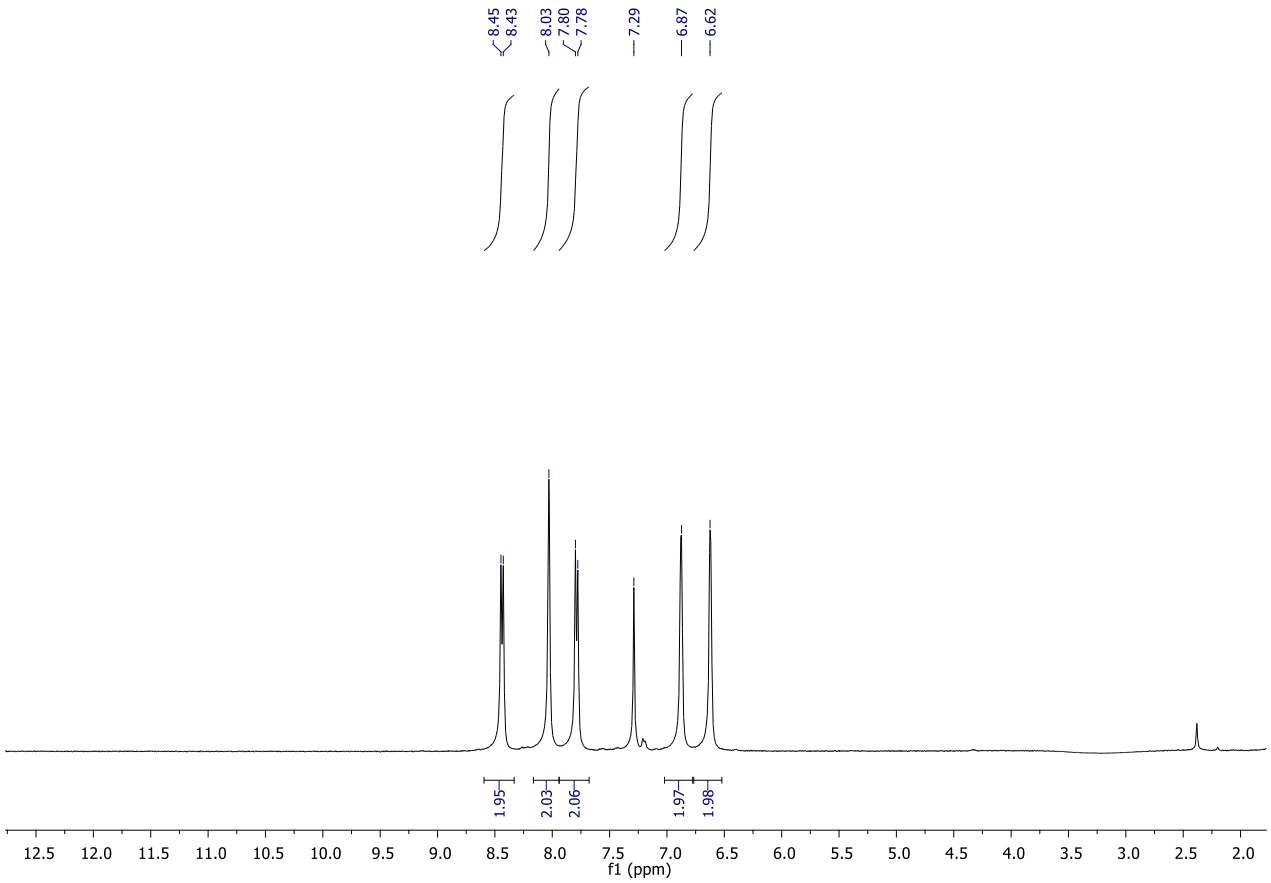


**Figure S15.** $^{1}$H NMR spectrum of **BDP-$NO_2$**.

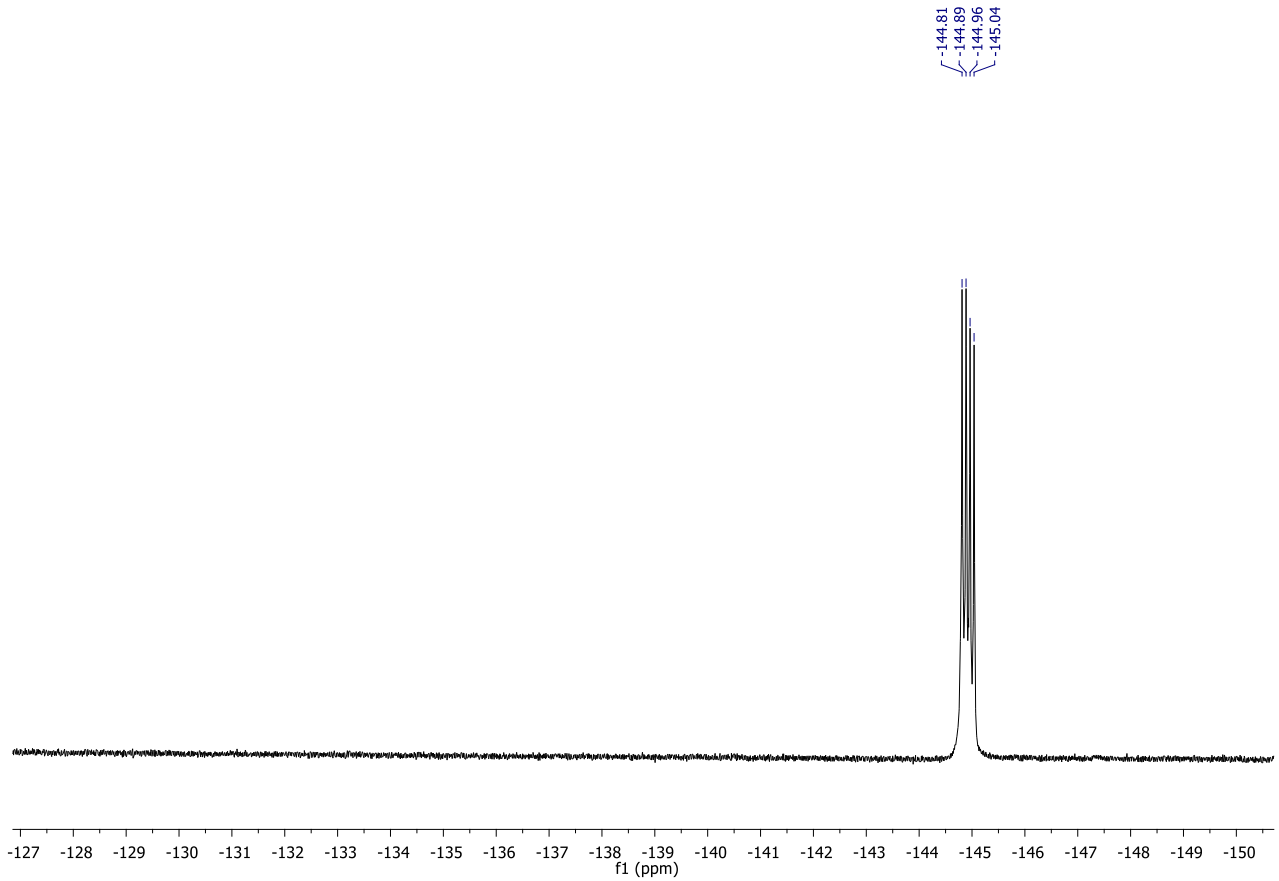


**Figure S16.** $^{19}$F NMR spectrum of **BDP-NO$_2$**.

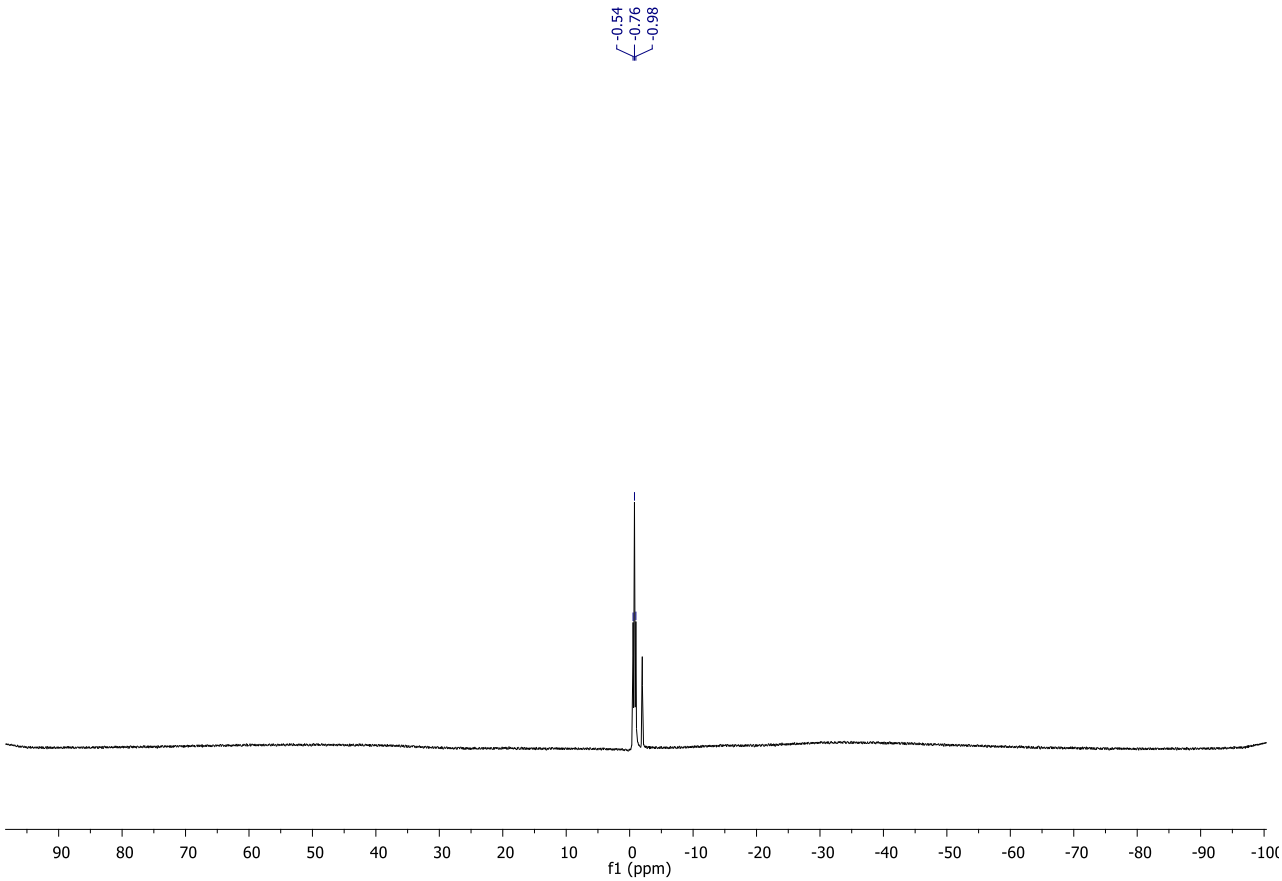


**Figure S17.** $^{11}$B NMR spectrum of **BDP-NO$_2$**.

## 5. List of references


1 H. L. Kee, C. Kirmaiery, L. Yu, P. Thamyongkit, W. J. Youngblood, M. E. Calder, L. Ramos, B. C. Noll, D. F. Bocian, W. R. Scheldt, R. R. Birge, J. S. Lindsey and D. Holten, *J. Phys. Chem. B*, 2005, **109**, 20433–20443.

2 M. R. Momeni and A. Brown, *J. Phys. Chem. A*, 2016, **120**, 2550–2560.

3 F. Li, S. I. Yang, Y. Ciringh, J. Seth, C. H. Martin, D. L. Singh, D. Kim, R. R. Birge, D. F. Bocian, D. Holten and J. S. Lindsey, *J. Am. Chem. Soc.*, 1998, **120**, 10001–10017.

4 A. Prlj, L. Vannay and C. Corminboeuf, *Helv. Chim. Acta*, 2017, **100**, 1–9.

5 C.-H. Lee and J. S. Lindsey, *Tetrahedron*, 1994, **50**, 11427–11440.

6 B. J. Littler, M. A. Miller, R. W. Wagner, C.-H. Hung, P. D. Boyle, D. F. O'Shea and J. S. Lindsey, *J. Org. Chem.*, 2002, **64**, 1391–1396.

7 C. Bruckner, V. Karunaratne, S. J. Rettig and D. Dolphin, *Can. J. Chem.*, 1996, **74**, 2182–2193.

8 C. Yu, L. Jiao, H. Yin, J. Zhou, W. Pang, Y. Wu, Z. Wang, G. Yang and E. Hao, *European J. Org. Chem.*, 2011, **2011**, 5460–5468.

9 A. C. Benniston, S. Clift and A. Harriman, *J. Mol. Struct.*, 2011, **985**, 346–354.